AD-A245 250

ION PAGE

Public
gathe
collec
Davis

age 1 hour per response, including the time for reviewing instructions, searching existing data source,
e collection of information. Send comments regarding this burden estimate or any other aspect of this
Washington Headquarters Services, Directorate for Information Operations and Reports, 1215 Jefferson
nagement and Budget, Paperwork Reduction Project (0704-0188), Washington, DC 20503.

1. A		3. REPORT TYPE AND DATES COVERED Reprint

4. TITLE AND SUBTITLE Title shown on Reprint	5. FUNDING NUMBERS $DAAL03-87-G-0004$

6. AUTHOR(S)

Author(s) listed on Reprint

7. PERFORMING ORGANIZATION NAME(S) AND ADDRESS(ES) Univ. of Nevada Las Vegas, Nevada 89154	8. PERFORMING ORGANIZATION REPORT NUMBER

9. SPONSORING/MONITORING AGENCY NAME(S) AND ADDRESS(ES) U. S. Army Research Office P. O. Box 12211 Research Triangle Park, NC 27709-2211	10. SPONSORING/MONITORING AGENCY REPORT NUMBER ARO 24960.68 MA-REP

11. SUPPLEMENTARY NOTES

The view, opinions and/or findings contained in this report are those of the author(s) and should not be construed as an official Department of the Army position, policy, or decision, unless so designated by other documentation.

12a. DISTRIBUTION/AVAILABILITY STATEMENT Approved for public release; distribution unlimited.	12b. DISTRIBUTION CODE

13. ABSTRACT (Maximum 200 words)

ABSTRACT ON REPRINT

DTIC
ELECTE
S   JAN 10 1992   D
D

14. SUBJECT TERMS		15. NUMBER OF PAGES
		16. PRICE CODE

17. SECURITY CLASSIFICATION OF REPORT UNCLASSIFIED	18. SECURITY CLASSIFICATION OF THIS PAGE UNCLASSIFIED	19. SECURITY CLASSIFICATION OF ABSTRACT UNCLASSIFIED	20. LIMITATION OF ABSTRACT UL

TECHNICAL PAPER

The Dynamic Response of a Flexible Three-Link Robot Using Strain Gages and Lagrange Polynomials

author

SAMAAN G. LADKANY, PH.D., P.E.
Professor—Civil Engineering
University of Nevada, Las Vegas
Las Vegas, Nevada

abstract

A method for modeling elastic robot kinematics is presented in this paper. The method uses the input of strain gages and joint encoders to determine the deflection of the links in in-plane and out-of-plane directions. Torsional flexures also are measured using strain rosettes. This information determines the end effector location which can be then used by the robot controller to damp the robot vibrations.

conference

92-00981

index terms

Robotics
Robots

INTRODUCTION

The objective of the Army Research Office (ARO) robotics project is to design and control a relatively lightweight elastic three-linked robot with defined paths of motion to carry an object load at least equal to its own weight. This study is supported at the University of Nevada, Las Vegas (UNLV) by the U.S. ARO under grant No. DAAL03-87-G-0004. A static and quasi dynamic mathematical model of the robot manipulator was derived [Ladkany, S.G. and Bonnoura, T.M, 1990] using the theory of structures and the fourth order differential equations of slender beams. The model gives the three displacements and the three rotations of the end effector due to static and quasi dynamic load vectors and moment vectors applied to the end effector and the centers of gravities of the links. The model was used in the design of the steel manipulator, the study of which is the subject of this research. It is believed that the results presented in this paper will expand existing robot kinematics and dynamic theory that include the effects of elasticity and active damping.

A major disadvantage in designing an elastic lightweight manipulator is the vibrational problems associated with the flexibility of the link members (Geradin and Berardin, 1984, Koren, 1985). In this research, link 2 & 3 of the thin, flexible steel robot are elastic and, therefore, subject to various modes of vibrations due to imposed loads. Because of the possible large amplitudes of vibration which may occur, active damping methods

control of the manipulator. To solve the vibrational problems, the use of active damping methods in conjunction with path-motion studies are under consideration in the design of the controller. The control technique concentrated on in this research, will be that of positioning strain gages at certain defined locations on each link in conjunction with angular encoder sensors at each joint to ultimately define kinematically the position of the end effector in space and time. The strain gages are connected to Wheatstone bridge amplification circuitry, which are connected in turn through an A-D board to micro-computers. The stain gage data and angular encoder sensor data are read into a FORTRAN program code utilizing Lagrange polynomials and shape functions developed to convert the strain gage readings and the angular encoder sensor readings into joint displacements. The axial, flexural, and rotational Lagrange polynomial displacement equations describe the deflected shape of each link in its local coordinate system as a function of the strain gage readings, their location x along the link, and time t. From the rotational displacement at a rigid joint, the rigid body rotation of the connected link is determined. Torsional displacements are determined from multiple strain gage elements known as rosettes. The rosettes are located on each link of the robotic model, and measure torsional shearing strain in the links caused by an external torque in the direction of the local axis of the link. A slight twist of torsional strain in one link will result in a rotational displacement of the joint connecting the two links. This, in turn, results in a rigid body out of plane rotation of the next link affecting the final location of the end effector. Once the local displacements are known, they are transformed into global displacements to be used by the controller.

Flexible Robot Manipulator Displacements

1. Displacement Equations Using Strain Gages and Lagrange Polynomials

The deflected and rotated position of the end effector in the global coordinate system required for ultimate control of the robot will be determined from the local deflections and rotations of links 2 & 3 and all associated rigid body motions of the manipulator arm (figures 5,6,7,8,9,&10). Strain gages are used to measure experimentally the maximum axial strains on all four orthogonal surfaces at three specific locations in the direction of the local ^ix-axis of link 2 and link 3. It is to be noted that strains measured along the faces of links 2 and 3, due to flexural bending alone, are of opposite signs. By using the Lagrange interpolation formula, a shape function is developed from these strain measurements which directly describes the strain $^i\bar{\epsilon}_x$ at any point ^ix along the local ^ix-axis of each link. The bar - notation above the strain symbol ϵ, defines a typical individual strain value at a face of a particular link member. All strain values are considered positive if tensile in nature and negative if compressive in nature. The superscript i in the notation defines the link number as shown below:

$$i=2 \text{ for link 2 and 3 for link 3.} \tag{1}$$

Lagrange polynomials are used to describe the axial strain $^i\bar{\epsilon}_x$ and then to use these polynomials to develop displacement equations to describe the deflected shape of link 2 and 3 in their respective local coordinate systems. From these displacement equations, the displacements at the jointed ends of link 2 and link 3 are determined. The displacements of interest to be determined are: three translational ^iu, ^iv and ^iw, three rotational $^i\theta_x$, $^i\theta_y$ and $^i\theta_z$ and all rigid body motion effects associated with these displacements. The three translational displacements are in the direction of the ^ix, ^iy and ^iz local axes respectively (figure 5 & 6). The three rotational displacements are defined by the subscripts x, y, and z which indicate the local axes about which the rotational displacements occur (figure 5 & 6). After all local displacements for links 2 and 3 are determined, the position of the end effector in global coordinates X, Y, and Z are found by coordinate transformation.

It is to be noted that the strain and displacement polynomials developed here are a function of ^ix and time t, where ^ix is the dimension along the local ^ix-axis from the clamped end of the link, and t is a time parameter relative to a set initial time. In order to simplify all further notation, it is to be understood from this point on that all equations developed are a function of x and t.

The structural design of the robotic links [Ladkany/Bannoura, 1988] limited the maximum allowable stresses calculated, for the worst loading condition, to a value below the yield stress of the material. Therefore, all stress-strain beam equations which apply

within the elastic range of the material will be valid here. The stress-strain beam equations developed are based upon linearized theory and the following assumptions:

$$\epsilon = \frac{\sigma}{E}, \text{ (Hooke's law)} \tag{2}$$

$$\gamma = \frac{\tau}{G}, \text{ (Hooke's law for shearing strain)} \tag{3}$$

$$\epsilon = \frac{F}{AE}, \text{ (axial strain)} \tag{4}$$

$$\epsilon_{max} = \frac{Mc}{EI}, \text{ (bending strain)} \tag{5}$$

$$\gamma_{max} = \frac{M_x c}{JG}, \text{ (torsional strain)} \tag{6}$$

where:

ϵ	Indicates axial strain.
ϵ_{max}	Indicates maximum strain at the extreme fiber.
σ	Indicates axial stress.
γ	Indicates shear strain.
γ_{max}	Indicates maximum shearing strain at the extreme fiber.
τ	Indicates shear stress.
A	Cross-sectional Area.
c	Distance from the neutral axis to the extreme fiber of the beam.
E	Defines the Modulus of Elasticity.
F	Axial force.
G	Defines the Shearing Modulus of Elasticity.
I	Defines the Moment of Inertia of the beam cross section.
J	Defines the polar Moment of Inertia.
M	Defines the moment value about the y and z axis at the point under consideration.
M_x	Torsional Moment about local x-axis.

Link 2 and link 3 are connected to the manipulator via rigid joints; they deflect under loading in the orthogonal planes as cantilever beams clamped at one end in their respective local coordinate systems. As shown in (figure 1) link 2 is considered clamped at joint B and link 3 is considered clamped at joint 2, however, link 2 and 3 are hinged together in the $^ix^iy$ plane and rigidly attached together in the $^ix^iz$ plane. The local ^ix axis has an origin at joint B for link 2 and an origin at joint 2 for link 3. Based on this assumption the local boundary conditions at $^ix=0$ for link 2 and link 3 are noted below:

$$@ \ ^ix=0 \tag{7}$$

$$^iu_o=0, \ ^iv_o=0, \ ^iw_o=0, \ ^i\theta_{x_o}=0, \ ^i\theta_{y_o}=0, \ ^i\theta_{z_o}=0$$

The proper interfacing of the pertinent strain gage sets in imperative for calculation of the correct displacements at any point $^i x$ along link 2 and link 3. Therefore, the first part of this section is devoted to clarification of the locations and orientations of the strain gages employed. On each line (link 2 & 3) there are four sets of strain gages mounted (figure 2 and 3a & b). The first three sets on each link are made up of four single element gages, and the fourth set is made up of two three element rosette strain gages.

The first three sets have one gage mounted on each face of the steel tube at the same location $^i(x_j)$ from the clamped end. The general notation used in this thesis to define the first three strain gage sets is shown below:

$$
^i_j\{\epsilon_j\} = {}^i \begin{bmatrix} \epsilon_1 \\ \epsilon_2 \\ \epsilon_3 \end{bmatrix}_\ell \tag{8}
$$

where:

i   Defines the link number (i=2 or 3).

j   Refers to the strain gage sets 1,2 and 3 (figure 2 and 3a), where set 1 is at location $^i x_1$, set 2 is at location $^i x_2$, and set three is at location $^i x_3$.

ℓ Is an integer which refers to the correct strain gage combination from the positions noted (figure 3b).

Note:

     $\ell=1$ Combined strain gages readings from positions 1,2,3 & 4.

     $\ell=2$ Combined strain gage readings from positions 1 & 3.

     $\ell=3$ Combined strain gage readings from positions 2 & 4.

The forth set on each link has one rosette on the positive $^i y$-face and negative $^i y$-face of link 2 and 3 at an arbitrary location $^i x_4$ (figure 2 and 2a). The exact location of the fourth set is not required since the torsion strain is constant throughout the length of each link. The general notation used in this thesis to define the fourth strain gage set for link 2 and 3 is shown below:

$$
^i_\psi\{\epsilon_\psi\} = {}^i \begin{bmatrix} \epsilon_{\psi_1} \\ \epsilon_{\psi_2} \\ \epsilon_{\psi_3} \end{bmatrix} \tag{9}
$$

Where:

ψ Is an angle in the plane of the rosette (figure 4).

§   Refers to the strain gage combinations required for temperature compensation to be defined more clearly in section 1.4.

A general polynomial which describes the axial strain along the local x-axis is:

$$
^{i}\epsilon(x,t) = {}^{i}\epsilon_x = a_1 + a_2{}^i x + a_3{}^i x^2 + \ldots + a_n{}^i x^{n-1} \tag{10}
$$

In the analysis, Lagrange polynomials will be used to describe the deformed shape of the manipulator links 2 and 3 using the strain gages. If these polynomials are to describe the static

deformed shape of the links exactly, the polynomials must have an order at least equal to the highest order in ^ix required for the theoretical deflection equations associated with the desired loading condition. It is assumed that the highest degree loading condition the link members may experience is that of a uniform load q (such as their own weight per linear ^ix dimension), Which leads to a fourth order polynomial. In general, from beam theory for a uniform load condition, the displacement equation which results in the highest order in ^ix is the bending displacement equation, which is termed Δ. The theoretical bending displacement equation from beam theory for a cantilever beam, where x is measured from the clamped end, is noted below [AISC, 1980]:

$$\Delta = \frac{q(4^ixL^3 - 6^ix^2L^2 + 4^ix^3L - ^ix^4)}{24EI} \tag{11}$$

where:

L   Defines the length of a typical cantilever beam.

q   Defines a uniform distributed loading.

From the equation above it can be seen that a fourth order Lagrange polynomial in ^ix is required to exactly describe the static bending deformation of link No.2 and link No.3 for this type of loading condition. Beam curvature is defined as the second derivative of the displacement equation $^i\Delta$ with respect to ^ix. The beam curvature is related to the maximum axial strain $^i\epsilon_{xmax}$ along the local ^ix-axis at the extreme fiber of the link member as shown below:

$$\frac{d^{2i}\Delta}{d^ix^2} = \frac{M}{EI} = \frac{^2\sigma_{max}}{Eh} = \frac{^2\epsilon_{xmax}}{h} \tag{12}$$

where:

h   Defines the out-to-out dimension of the link member cross section.

σ_{max} Defines the maximum stress along the local x-axis at the extreme fiber of the steel tube.

In order to determine the exact static displacement equation $^i\Delta$, a Lagrange polynomial which describes the strain must be at least second order in ^ix (n=3). by integrating twice, the second order strain polynomial in ^ix becomes a fourth order polynomial in ^ix and thus defines the displacement equation $^i\Delta$. The Lagrange polynomial required to develop all of the displacement equations desired here is:

$$^{i-}\epsilon_x = {}^ia_1 + {}^ia_2{}^ix + {}^ia_3{}^ix^2 \tag{13}$$

To derive a second order polynomial in ^ix, that defines the strain as a shape function, a Lagrange polynomial is used in terms of the strain values. Lagrange's interpolation formula [Cook, 1981] used to define the axial strain $^{i-}\epsilon_x$ as a polynomial in terms of a shape function $^i\lfloor N \rfloor$ is noted below:

$$^{i-}\epsilon_x = {}^i\lfloor N \rfloor {}^i_\ell(\epsilon_j) \tag{14}$$

where:

The strain values $^i_\ell(\epsilon_j)$ as defined above in equation (8) are strain measurements determined experimentally by placing three single element strain gages orientated along the local ^{i}x-axis of each link (figure 2 and 3a) and located at $^ix_1$, $^ix_2$ and $^ix_3$ respectively. The values $^ix_1$, $^ix_2$ and $^ix_3$ are set dimensions, measured from the clamped end of each link (figure 2 and 3a). By using the Lagrange polynomial (14) in conjunction with the equations defining the small deflection theory of beams, other polynomials are derived which describe the axial, rotational, torsional and flexural displacements of each link. The shape function $^i\lfloor N \rfloor = {^i}\lfloor N_1 N_2 N_3 \rfloor$ used in the Lagrange polynomials are formulated below:

$$^iN_1 = \frac{(^ix - {^i}x_2)(^ix - {^i}x_3)}{(^ix_1 - {^i}x_2)(^ix_1 - {^i}x_3)} \tag{15}$$

$$^iN_2 = \frac{(^ix - {^i}x_1)(^ix - {^i}x_3)}{(^ix_2 - {^i}x_1)(^ix_2 - {^i}x_3)}$$

$$^iN_3 = \frac{(^ix - {^i}x_1)(^ix - {^i}x_2)}{(^ix_3 - {^i}x_1)(^ix_3 - {^i}x_2)}$$

1.1 Axial Displacements In Local ^{i}x Direction

The required combination of strain gage readings ($\ell=1$), for the determination of the axial displacement ^{i}u are shown below:

$$^i_1(\epsilon_j) = {^i_1}\left[\frac{\overline{\epsilon}_1 + \overline{\epsilon}_2 + \overline{\epsilon}_3 + \overline{\epsilon}_4}{4} \right]_j \tag{16}$$

$$(i=2,3)$$
$$(j=1,2,3)$$

In this equation, the individual single element strain gage values which make up the strain gage set at location $^i(x_j)$ are further described as:

$^{i\cdot}\epsilon_1$ [positive y face position 1 (figure 3b)]
$^{i\cdot}\epsilon_2$ [positive z face position 2 (figure 3b)]
$^{i\cdot}\epsilon_3$ [negative y face position 3 (figure 3b)]
$^{i\cdot}\epsilon_4$ [negative z face position 4 (figure 3b)]

From equation (15) the axial displacement ^{i}u, determined from the strain measurements $^i_1(\epsilon_j)$, is obtained by integration:

$$^{i\cdot}\epsilon_x = \frac{d^iu}{d^ix} = {^i}\lfloor N \rfloor {^i_1}(\epsilon_j) \tag{17}$$

Therefore:

$$^iu = {^i_1}(\epsilon_j)\int_x {^i}\lfloor N \rfloor dx = {^i}b_1 + {^i}b_2 {^i}x + {^i}b_3 {^i}x^2 + {^i}b_4 {^i}x^3$$

1.2 Flexural Displacements In Local $^i y$ Direction

The required combination of strain gage readings ($\ell=2$) for the determination of the flexural $^i v$ displacements is shown below:

$$^i_2\{\epsilon_j\} = ^i_2\left[\frac{\overline{\epsilon}_3 - \overline{\epsilon}_1}{2}\right]_j \tag{18}$$

$$(i=2,3)$$
$$(j=1,2,3)$$

where:

$^{i\cdot}\epsilon_1$ [positive y face position 1 (figure 3b)]
$^{i\cdot}\epsilon_3$ [negative y face position 3 (figure 3b)]

The bending strain varies with the bending moment which varies along the length of the link, therefore, the bending strain is determined at each $^i(x_j)$ from the strain gages. From equation (15) the flexural displacements $^i v$ are obtained by integration:

$$\frac{d^2\,^i v}{d^i x^2} = \frac{2}{h}\,^i\lfloor N\rfloor\,^i_2\{\epsilon_j\} \tag{19}$$

where:

$$^i v = \frac{2}{h}\,^i_2(\epsilon_j)\int_x\int_x{}^i\lfloor N\rfloor\,dxdx = {}^i c_1 + {}^i c_2{}^i x + {}^i c_3{}^i x^2 + {}^i c_4{}^i x^3 + {}^i c_5{}^i x^4$$

or

$$^i v = \frac{2}{h}\left\{\left[\frac{\dfrac{^i x^4}{12} - \dfrac{^i x^3({}^i x_2 + {}^i x_3)}{6} + {}^i x_2\,{}^i x_3\dfrac{{}^i x^2}{2}}{({}^i x_1 - {}^i x_2)({}^i x_1 - {}^i x_3)}\right]{}^i_2\epsilon_1\right.$$

$$+\left[\frac{\dfrac{^i x^4}{12} - \dfrac{^i x^3({}^i x_1 + {}^i x_3)}{6} + {}^i x_1\,{}^i x_3\dfrac{{}^i x^2}{2}}{({}^i x_2 - {}^i x_1)({}^i x_2 - {}^i x_3)}\right]{}^i_2\epsilon_2$$

$$\left.+\left[\frac{\dfrac{^i x^4}{12} - \dfrac{^i x^3({}^i x_1 + {}^i x_2)}{6} + {}^i x_1\,{}^i x_2\dfrac{{}^i x^2}{2}}{({}^i x_3 - {}^i x_1)({}^i x_3 - {}^i x_2)}\right]{}^i_2\epsilon_3\right\} \tag{20}$$

$$+ c_3{}^i x + c_4$$

From the boundary conditions at x=0, the constants of integration ($C_3=C_4=0$) are obtained.

It should be again noted that the fourth order polynomial derived above will exactly describe the static deflected shape of each robotic link with applied concentrated loads and reaction couples as well as uniformly distributed loadings. Flexural

displacements in the local ^iz are derived in a similar manner.

1.3 Torsional Rotational Displacements In Local ^ix Direction

A torque applied to a link will induce a shearing strain in that link. The links, made of structural steel tubing, are considered thin walled tubes. For thin walled tubes of constant thickness, the shearing strain due to applied concentrated torques is constant for the full length of each link. To determine the shearing strain, two rosette strain gages are mounted, one on the positive y-face and one on the negative y-face of each link at location ^ix_l (figure 2 & 3a). It should be noted that mounting rosettes on the positive and negative z-faces would also give the same results. Each rosette is a cluster of three single element strain gages oriented in the local $^ix^iz$ plane at angles $^i\psi_1$, $^i\psi_2$, and $^i\psi_3$ (figure 4). Opposite face single element strain gages in each rosette are oriented in the same directions. Two rosettes per link i are necessary to temperature compensate and properly determine the torsional shearing strain. The strain at any arbitrary angle in two dimensional space on the surface of the steel tube is defined in terms of the local cartesian strains as shown below [Popov, 1952]:

$$^i\epsilon_\psi = {}^i\epsilon_x\cos^2({}^i\psi) + {}^i\epsilon_z\sin^2({}^i\psi) + {}^i\gamma_{xz}\sin{}^i\psi\cos{}^i\psi \qquad (21)$$

$$(i=2,3)$$

where:

$^i\psi$ Is defined as an arbitrary angle measured from the ^ix axis (figure 4).

For a three element strain gage cluster or rosette, three simultaneous equations may be written to describe the strain in each strain gage element for each corresponding angle $^i\psi_1$, $^i\psi_2$, and $^i\psi_3$.

The strain values $^i\epsilon_{\psi 1}$, $^i\epsilon_{\psi 2}$, and $^i\epsilon_{\psi 3}$ are determined experimentally from the strain gages and, therefore, are known values. To minimize computational work, three element rosette gages with $^i\psi_1=0^0$, $^i\psi_2=45^0$, and $^i\psi_3=90^0$ were chosen for the laboratory model. This type of rosette is also known as a rectangular or 45° strain rosette. By direct substitution of $^i\psi_1=0^0$, $^i\psi_2=45^0$, and $^i\psi_3=90^0$; $^i\epsilon_x$, $^i\epsilon_z$, and $^i\gamma_{xz}$ are determined as shown below for a rectangular rosette:

$$^i\epsilon_{\psi 1} = {}^i\epsilon_x \qquad (22)$$
$$^i\epsilon_{\psi 3} = {}^i\epsilon_z \qquad (23)$$
$$^i\gamma_{xz} = 2{}^i\epsilon_{\psi 2} - ({}^i\epsilon_{\psi 1} + {}^i\epsilon_{\psi 3}) \qquad (24)$$

From the torsional shear strain $^i\gamma_{xz}$, the rotational displacements $^i\theta_x$ are determined in the local coordinate system as shown below:

$$^i\theta_x = \frac{2L^i}{h}{}^i\gamma_{xz} = \frac{2L^i}{h}\left\{2{}^i\epsilon_{\psi 2} - ({}^i\epsilon_{\psi 1} + {}^i\epsilon_{\psi 3})\right\} \qquad (25)$$

1.4 Rotational Bending Displacements In Local iy Direction

The required combination of strain gage readings ($\ell=3$), for the determination of the rotational $-{}^i\theta_y$ and ^iw displacement is

shown below:

$$i_3(\epsilon_j) = {}^i\left[\frac{\overline{\epsilon}_4 - \overline{\epsilon}_2}{2}\right]_j$$
(26)

$$(i=2,3)$$
$$(j=1,2,3)$$

where:

$i^-\epsilon_2$ [positive z face position 2 (figure 3b)]

$i^-\epsilon_4$ [negative z face position 4 (figure 3b)]

The rotational displacements $-{}^i\theta_y$ derived from the strain measurements ${}^i_3(\epsilon_j)$ are defined below. The negative sign in front is required for consistency with the right-hand rule sign convention.

$$-{}^i\theta_y = \frac{d^iw}{d^ix} = {}^i_3(\epsilon_j)\int_x {}^i[N]\,dx$$
(27)

where:

$$-{}^i\theta_y = {}^if_1 + {}^if_2\,{}^ix + {}^if_3\,{}^ix^2 + {}^if_4\,{}^ix^3$$

or

$$-{}^i\theta_y = \frac{2}{h}\left[\left[\frac{{}^ix^3 - {}^ix^2({}^ix_2 + {}^ix_3) + {}^ix_2\,{}^ix_3\,{}^ix}{2}}{({}^ix_1 - {}^ix_2)({}^ix_1 - {}^ix_3)}\right]{}^i_3\epsilon_1\right.$$
(28)

$$+ \left[\frac{\frac{{}^ix^3 - {}^ix^2({}^ix_1 + {}^ix_3) + {}^ix_1\,{}^ix_3\,{}^ix}{2}}{({}^ix_2 - {}^ix_1)({}^ix_2 - {}^ix_3)}\right]{}^i_3\epsilon_2$$

$$\left.+ \left[\frac{\frac{{}^ix^3 - {}^ix^2({}^ix_1 + {}^ix_2) + {}^ix_1\,{}^ix_2\,{}^ix}{2}}{({}^ix_3 - {}^ix_1)({}^ix_3 - {}^ix_2)}\right]{}^i_3\epsilon_3\right] + C_2$$

From the boundary conditions at x=0, the constant of integration (C_2=0) is obtained. Rotational bending displacements in the local ${}^i\overline{z}$ direction is derived in a similar manner.

2. Joint Displacements
2.1 Joint Displacement Notations

The displacement equations developed using the Lagrange polynomials exactly describe the static deflected shape of link 2 and 3, as previously noted. In order to determine the deflected and rotated position of the end effector, all joint displacements and all rigid body motion displacements must be determined. The joint displacements at the ends of link 2 and 3 in the local coordinate systems can be determined from the displacement equations developed.

Special notations are required to help clarify the many local

displacements at each joint analyzed in this and the following subsections. Where, for example, $_{\iota}^{i}v_{s}$ corresponds to the displacement in the ^{i}y direction at joint i for condition s (s=1,2,3...6).

i   Defines the link number.

ι Defines the joint number at which the displacements are determined (ι= 2, 3,or 4).

s   Is a displacement designation developed to simplify programming notation and to allow for a method of separately calculation displacements due to rigid body motions where:

    s=1 For the displacements determined from the strain gage values.

    s=2 For the displacements from rigid body motions in the $^{i}x^{i}y$ plane.

    s=3 For the displacements from rigid body motions in the $^{i}x^{i}z$ plane.

    s=4 For the displacements from rigid body motions from rotational displacements equations $^{i}\theta_{x}$, $^{i}\theta_{y}$, and $^{i}\theta_{z}$.

    s=5 For the displacements from rigid body motions from actuator fluctuations.

In order to find joint displacements $_{\iota}^{i}u_{1}$, $_{\iota}^{i}v_{1}$, $_{\iota}^{i}w_{1}$, $_{\iota}^{i}\theta_{y1}$, $_{\iota}^{i}\theta_{z1}$ the length L_{1} of link i must be substituted for the ^{i}x terms in the displacements equations in addition to inputting the set location values $_{\iota}^{i}(x_{j})$ and the strain gage combination values $_{\iota}^{i}(\epsilon_{j})$. To find the remaining joint displacements $_{\iota}^{i}\theta_{x1}$ the length L_{1} of link i, the out to out dimension of the link h, and the strain values $^{i}(\epsilon_{\bullet\bullet})$ are substituted into equation (25).

2.2 Rigid Body Motion From Joint Displacements

Rigid body motion effects (RBME) are translational displacements and rigid body rotational displacements resulting from adjoining link joint displacements. All articulated robot manipulators of more than one link experience rigid body motions which are a function of the number of degrees of freedom of each joint. It is to be understood that the rigid body effects are first determined in the local coordinate system and then transformed to the global coordinate system before being combined with other global displacements.

2.3 Rigid Body Motion Effects In The Local $^{i}x^{i}y$ Plane

The RBME in the local xy plane result from the joint displacements $_{2}^{2}v_{1}$, $_{3}^{3}v_{1}$, and $_{3}^{3}\theta_{z1}$ at joint 2 and 3. Joint 2 is considered pinned in the local and global XY plane. Therefore, any flexural displacement $_{2}^{2}v_{1}$ at joint 2 results in only a rigid body translation of joint 3 and end effector center point (EECP) 4 (figure 7). Similarly, a flexural displacement $_{3}^{3}v_{1}$ at joint 3 will result in a rigid body translation of EECP 4. However, since joint 3 is rigid in the global XY plane, the rotational displacement $_{3}^{3}\theta_{z1}$ which accompanies the flexural displacement $_{3}^{3}v_{1}$ at joint 3 results in an additional rotation of the end effector link and ultimately

a change in the position of EECP 4. It is to be noted that there are no out of plane RBME associated with these particular displacements. Therefore, The displacements in the ^iz direction are not indicated in this section.

A positive flexural joint displacement $^2_2v_1$ at the end of link 2 at joint 2 causes joint 2 to move to 2', joint 3 to move to 3', and joint 4 to move to 4', (figure 7). This represents RBME in translation of joint 3 and joint 4 as defined below:

$$_3u' = \,^2_2v_1\sin(\phi_2-\phi_1) \tag{29}$$

$$_3v' = \,^2_2v_1\cos(\phi_2-\phi_1) \tag{30}$$

$$_4u' = \,^2_2v_1\sin(\phi_3-\phi_1) \tag{31}$$

$$_4v' = \,^2_2v_1\cos(\phi_3-\phi_1) \tag{32}$$

where the superscript 4 indicates the local rigid body displacements at the EECP 4.

A positive flexural displacement $^3_3v_1$ at the end of link 3 at joint 3 causes the joint at 3' to move to 3" and the EECP 4' to move to 4" (figure 3). This represents RBME in translation of EECP 4 as defined below:

$$_4u'' = \,^3_3v_1\sin(\phi_3-\phi_2) \tag{33}$$

$$_4v'' = \,^3_3v_1\cos(\phi_3-\phi_2) \tag{34}$$

Since joint 3 is considered rigid in the $^ix^iy$ plane, a rotational displacement $^3_3\theta_{z1}$ at the end of link 3 at joint 3 results in RBME in rotation of the end effector link (figure 7). As joint 3 rotates an angle $^3_3\theta_{z1}$ EECP 4" moves to 4"' (figure 7) and a rigid body rotation of the EECP 4 also occurs. These displacements are defined below:

$$_4u''' = -L_4\,^3_3\theta_{z1}\sin(^3_3\theta_{z1}/2) \tag{35}$$

$$_4v''' = L_4\,^3_3\theta_{z1}\cos(^3_3\theta_{z1}/2) \tag{36}$$

$$_4\theta_z''' = \,^3_3\theta_{z1} \tag{37}$$

The total net RBME which result at joint 3 and EECP 4 from the displacements $^2_2v_1$, $^3_3v_1$, and $^3_3\theta_{z1}$ are combined below:

$$^3_3u_1 = \,_3u' \tag{38}$$

$$^3_3v_1 = \,_3v' \tag{39}$$

$$^4_4u_2 = \,_4u' + \,_4u'' + \,_4u''' \tag{40}$$

$$^4_4v_2 = \,_4v' + \,_4v'' + \,_4v''' \tag{41}$$

$$^4_4\theta_{z2} = \,_4\theta_z''' \tag{42}$$

Similar derivations are made for the rigid body motion effects in the $^ix^iz$ plane.

2.4 Rigid Body Motion Effects From Rotational Displacements $^i_\ell\theta_{xs}$

The local rotational displacements $^i_\ell\theta_x$ result from torsional moments and all components of those moments and forces which cause a twisting deformation in link 2 and 3. A local rotational displacement $^2_2\theta_{x1}$ or twist in link 2 at joint 2 will result in a rotational RBME in link 3 and also in the end effector link. A local rotational displacement $^3_3\theta_{x1}$ or twist in link 3, by the same reasoning, will result in a rotational RBME in the end effector link. The RBME associated with these rotational displacements are described separately below:

As joint 2 rotates the angular displacement $^2_2\theta_{x1}$ joint 3 moves to 3', which results in the displacements $_3u'$, $_3v'$, and $_3w'$ at joint 3 and a rigid body rotation $_3\theta_x'$ (figure 9). In addition, as joint 2 rotates the angular displacement $^2_2\theta_{x1}$ end effector center point (EECP) 4 moves to 4', which results in the displacements $_4u'$, $_4v'$, and $_4w'$ at EECP 6 and a rigid body rotation $_4\theta_x'$ (figure 9). A few of the displacements relating to this motion are described below:

$$_3u' = R_2\sin(\phi_2-\phi_1) \qquad (43)$$

$$_3\theta_x' = {}^2_2\theta_{x1}\cos(\phi_2-\phi_1) \qquad (44)$$

where:

$$R_2 = R_1(\cos({}^2_2\theta_{x1})-1.0) \qquad (45)$$

As joint 3 rotates the angular displacement $^3_3\theta_{x1}$ EECP 6' moves to 6" which results in the displacements $_4u''$, $_4v''$, and $_4w''$ in addition to a rigid body rotation $_4\theta_x''$ at EECP 4 (figure 10). A few of the displacements relation to this motion are described below:

$$_4u'' = R_6\sin(\phi_3-\phi_2) \qquad (46)$$

$$_4\theta_x'' = {}^3_3\theta_{x1}\cos(\phi_3-\phi_2) \qquad (47)$$

where:

$$R_6 = R_5(\cos({}^3_3\theta_{x1})-1.0) \qquad (48)$$

In summary, the net effect at the end effector in local coordinates at the EECP 4 from the RBME associated with the rotational displacements $^i\theta_x$ are:

$$^3_3u_4 = {}_3u' \qquad (49)$$

$$^3_3v_4 = {}_3v' \qquad (50)$$

$$^3_3w_4 = {}_3w' \qquad (51)$$

$$^3_3\theta_{x4} = {}_3\theta_x' \qquad (52)$$

$$^4_4u_4 = {}_4u' + {}_4u'' \qquad (53)$$

$$^4_4v_4 = {}_4v' + {}_4v'' \qquad (54)$$

$$^4_4w_4 = {}_4w' + {}_4w'' \qquad (55)$$

$$^4_4\theta_{x4} = {}_4\theta_x' + {}_4\theta_x'' \qquad (56)$$

2.5 Rigid Body Motion Effects From Actuator Fluctuations

Any fluid displacement in the hydraulic actuators ab and de on the model (figure 1) will induce a rigid body motion effect at joints 2, 3 and the end effector center point (EECP) 4. Any fluid displacement in the hydraulic actuator at the base link 1 is neglected here, therefore, all out-of-plane displacements ${}^i_1 w_s$ are zero and not shown.

The displacements from actuator ab are determined and defined as displacements ${}^i_1 u_s$, and ${}^i_1 v_s$ at joints 2,3 and EECP 4. This derivation is shown below (figure 11):

$$d\varphi = \frac{C_1 EER_1}{A_1 B_1 \sin\varphi} = d\Phi_1 \tag{57}$$

where:

$$\varphi = \frac{\pi + \Phi_1 - \phi}{2} \tag{58}$$

$$C_1 = [A_1^2 + B_1^2 - 2A_1 B_1 \cos\varphi]^{1/2} \tag{59}$$

where:

EER_1 Fluid displacements in units of strain in actuator ab.
$B1$ Dimension (figure 11).
ϕ Set angle equal to $\tan^{-1}(6"/22") = .26625$ radians (figure 11).

The fluid displacements from actuator de are determined and defined as displacements ${}^i_1 u_s$ and ${}^i_1 v_s$ at joints 2,3 and EECP 4. This derivation is shown below (figure 11):

$$d\varphi = \frac{C_2 EER_2}{A_2 B_2 \sin\varphi} = d\Phi_2 \tag{60}$$

$$C_2 = [A_2^2 + B_2^2 - 2A_2 B_2 \cos\varphi]^{1/2} \tag{61}$$

$${}_3 u' = L_3 d\alpha \sin(d\alpha/2) \tag{62}$$

The other displacements are derived in a similar manner.

Where:

ERR_2 Fluid displacements in units of strain in actuator de.
λ Angle at joint 2 set at $126.87° = 2.214$ radians (figure 11).

The combined displacements due to the fluid displacements in actuators ab and de at joints 2 and 3 and the EECP 4 are:

$${}^2_2 u_5 = {}_2 u' \tag{63}$$

$${}^2_2 v_5 = {}_2 v' \tag{64}$$

$${}^3_3 u_5 = {}_3 u' + {}_3 u'' \tag{65}$$

$${}^3_3 v_5 = {}_3 v' + {}_3 v'' \tag{66}$$

$${}^4_4 u_5 = {}_4 u' + {}_4 u'' \tag{67}$$

$${}^4_4 v_5 = {}_4 v' + {}_4 v'' \tag{68}$$

2.6 Summary of Joint Displacements

In summary, the joint displacements at the ends of link 2 and 3 in the local coordinate systems can combined with all additional local joint displacements due to rigid body motion effects as shown below:

$$_{\iota}^{i}u = \sum_{s=1}^{6} {}_{\iota}^{i}u_{s} \qquad (69)$$

$$_{\iota}^{i}\theta_{x} = \sum_{s=1}^{6} {}_{\iota}^{i}\theta_{s} \qquad (70)$$

$$(\iota = 2,3,4)$$

Other displacements are summed in the same manner.

3. Local to Global Coordinate Transformations

To be of use to the controller, the local displacements determined in the above discussion need to be combined and then transformed from the local coordinate systems to the global coordinate systems, before combining with any additional global displacements, in order to determine the location of the end effector. Upper case notation is used to define the global displacements and lower case notation is used to define the local displacements (figure 5 & 6).

$$
\begin{bmatrix} U \\ V \\ W \\ \theta_X \\ \theta_Y \\ \theta_Z \end{bmatrix}
=
\begin{bmatrix}
C & -S & 0 & 0 & 0 & 0 \\
S & C & 0 & 0 & 0 & 0 \\
0 & 0 & 1 & 0 & 0 & 0 \\
0 & 0 & 0 & C & -S & 0 \\
0 & 0 & 0 & S & C & 0 \\
0 & 0 & 0 & 0 & 0 & 1
\end{bmatrix}
\cdot
\begin{bmatrix} u \\ v \\ w \\ \theta_x \\ \theta_y \\ \theta_z \end{bmatrix}_{\iota}^{i}
\qquad (71)
$$

where:

C   Cosine of joint angle $\phi_{\iota} [\cos(\phi_{\iota})]$.
S   Sine of joint angle $\phi_{\iota} [\sin(\phi_{\iota})]$.
ι Defines the joint number (2, 3, or 4).

4. The Experimental Setup

The strain gages have been mounted on the robot and tested under static loading conditions. The measured displacements of the end effectors are within 2-3% of the computed displacements using the output of the strain gages. A dynamic data acquisition system capable of 1000 scans per second is being tested for active on line control of the robot.

5. Conclusion

The dynamic response of a three-link flexible robot using sets of strain gages and rosettes has been for mulated and Lagrange polynomials are used in the analyses to interpolate a strain field and then integrate it to obtain the 3-D displacements and rotations of the joint. Geometrical expressions were derived to sum up all flexibility and rigid body motions to predict the actual displacements of the end effector.
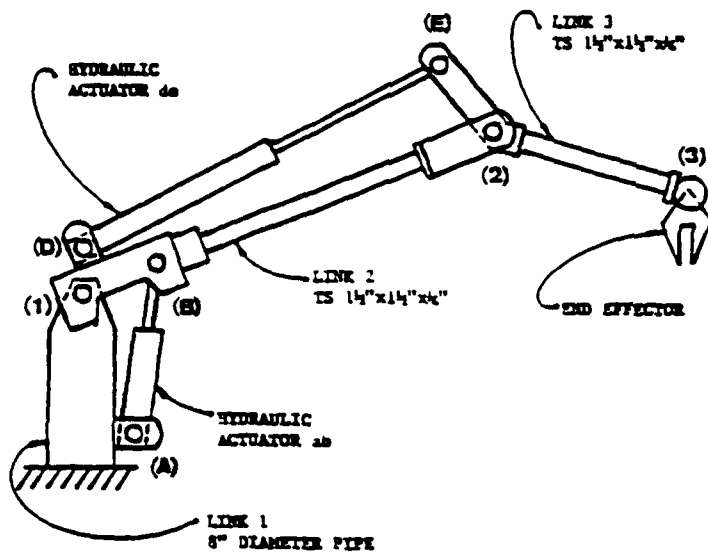
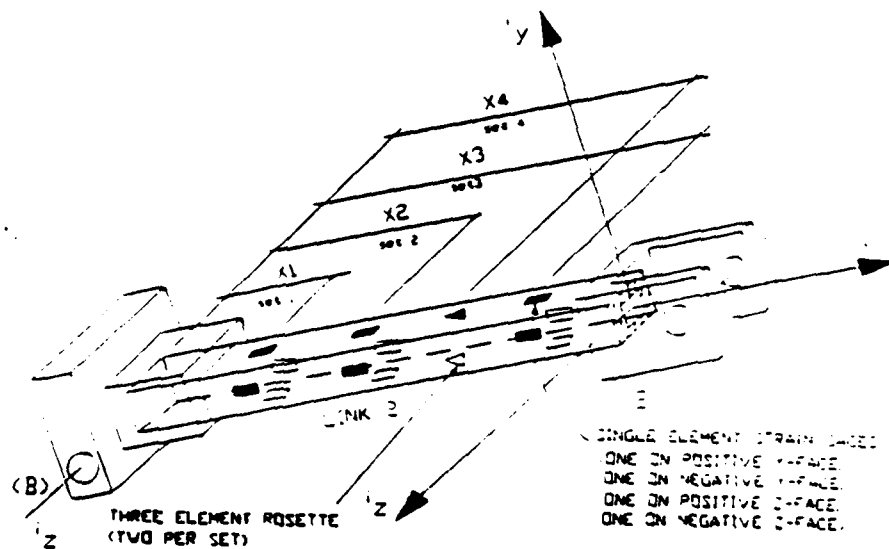FIGURE 1: SCHEMATIC OF THREE-LINK ROBOT MANIPULATOR
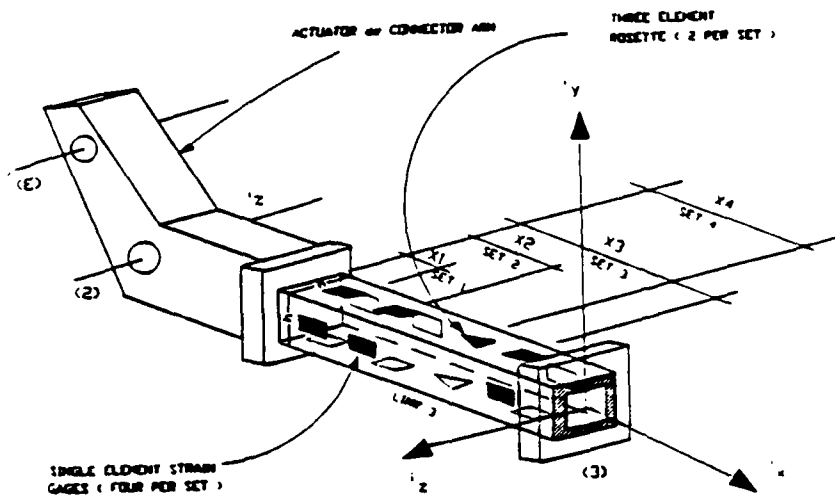

FIGURE 2: LINK 2 STRAIN GAGE SET LOCATIONS

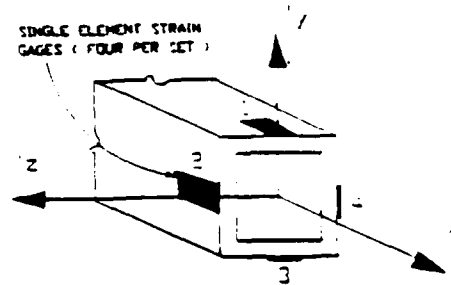FIGURE 3a: LINK 3 STRAIN GAGE SET LOCATIONS

FIGURE 3b: SINGLE ELEMENT STRAIN GAGE POSITIONS

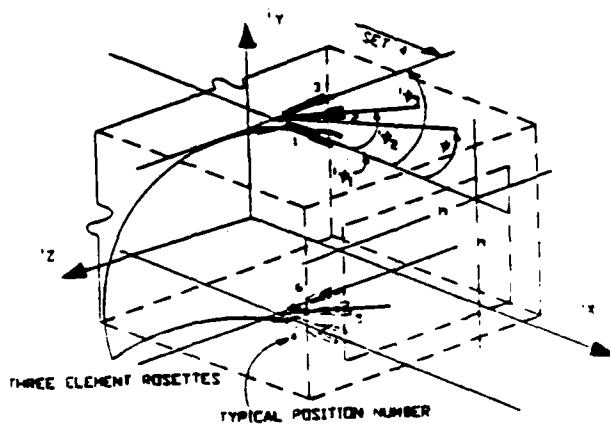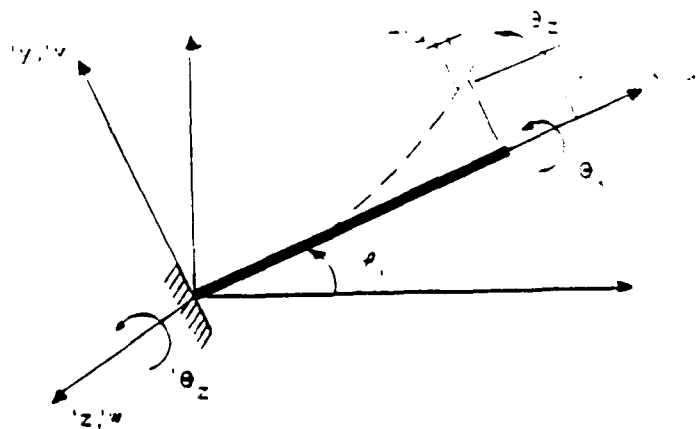FIGURE 4: THREE ELEMENT ROSETTE ORIENTATION
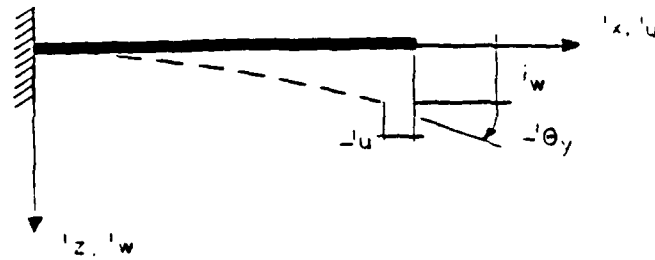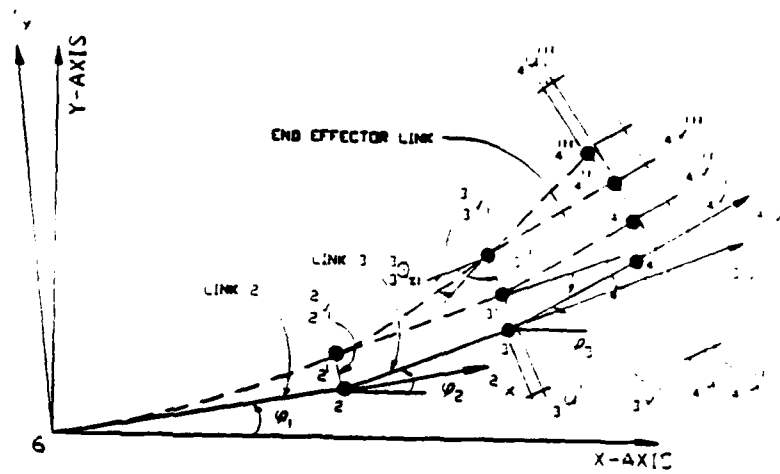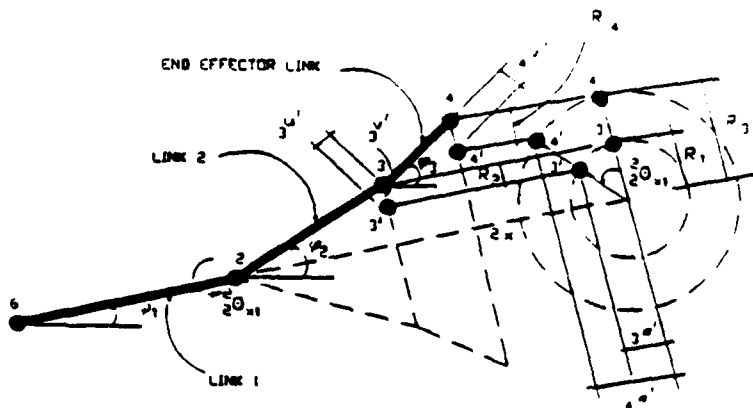
FIGURE 5: LINK ELEVATION VIEW AS A CANTILEVER BEAM

FIGURE 6: LINK PLAN VIEW AS A CANTILEVER BEAM

FIGURE 7: RIGID BODY MOTION EFFECTS IN 'X'Y PLANE
(REFER TO EQUATIONS 37 THROUGH 40)

FIGURE 8: RIGID BODY MOTION EFFECTS FROM ROTATIONAL DISPLACEMENT
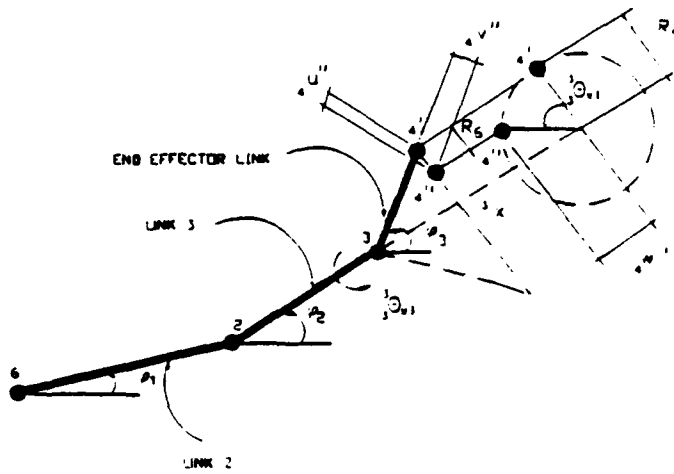(REFER TO EQUATIONS 45 THROUGH 48)

FIGURE 9: RIGID BODY MOTION EFFECTS FROM ROTATIONAL DISPLACEMENT
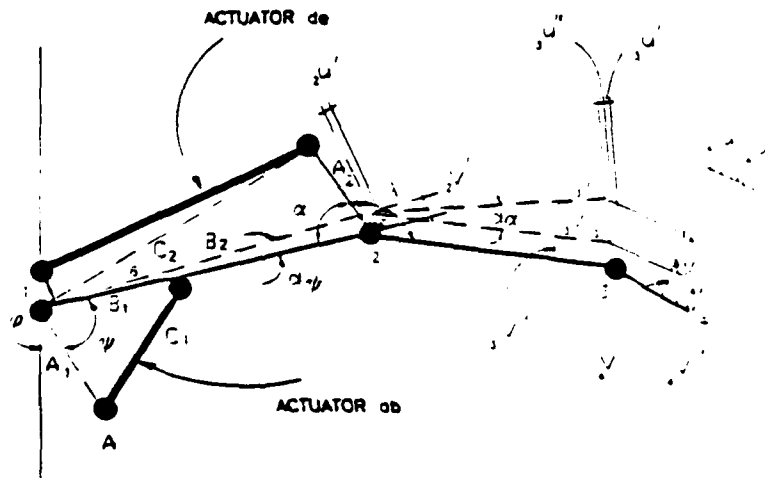(REFER TO EQUATIONS 45 THROUGH 48)

FIGURE 10: RIGID BODY MOTION EFFECTS FROM ACTUATOR FLUCTUATIONS
(REFER TO EQUATIONS 60 THROUGH 62)

REFERENCES:

Cook, R. D., 1981, <u>Concepts and Application of Finite Element Analysis</u>, Second Edition, John Wiley and Sons, Inc., New York.

Culbreth, W.G., and Krueger, A., 1989, "Computer Simulation of a Three-Link Hydraulically Actuated Robotic Arm", Society of Manufacturing Engineers Transaction, May 7-11.

Dally, J.W. and Riley, W.F., 1965, <u>Experimental Stress Analysis</u>, McGraw-Hill Book Company, Inc., New York.

Geradin, M., Rober, G., Bernardin, C., 1984, "Dynamic Modelling of Manipulators With Flexible Members", Advanced Software in Robotics, Elsevier Science Publishers B.V. (North Holland), pp. 27-39.

Koren, Yoram., 1985, <u>Robotics For Engineers</u>, McGraw-Hill Book Company, Inc., New York.

Ladkany, S.G. and Bannoura, T.M., 1989, "Structural Design of a Flexible Three-Link Hydraulically Activated Robotic Arm", Society of Manufacturing Engineers Transaction, May 7-11.

Trabia, M.B. and Yim, W., 1989, "Dynamic Simulation of a Three Degrees of Freedom Hydraulically Activated Robotic Arm with Flexible Links, Society of Manufacturing Engineers Transaction, May 7-11.